
Article:
Zhang, S, Planavsky, NJ, Krause, AJ orcid.org/0000-0002-9771-8101 et al. (2 more authors) (2018) Model based Paleozoic atmospheric oxygen estimates: a revisit to GEOCARBSULF. American Journal of Science, 318 (5). pp. 557-589. ISSN 0002-9599

https://doi.org/10.2475/05.2018.05

MODEL BASED PALEOZOIC ATMOSPHERIC OXYGEN ESTIMATES: A REVISIT TO GEOCARBSULF

Shuang Zhang[1*], Noah J. Planavsky[1], Alexander J. Krause[2], Edward W. Bolton[1], and Benjamin J. W. Mills[2]

[1] Department of Geology and Geophysics, Yale University, New Haven, Connecticut 06520, USA

[2] School of Earth and Environment, University of Leeds, Leeds LS2 9JT, UK

[*] Corresponding author email: shuang.zhang@yale.edu

Keywords: Atmospheric O_2; GEOCARBSULF; Paleozoic; Carbonate isotope; Plant evolution

Abstract. Geological redox proxies increasingly point toward low atmospheric oxygen concentrations during the early Paleozoic Era, and a protracted rise towards present-day levels. However, these proxies currently provide qualitative estimates of atmospheric O_2 levels. Global biogeochemical models, in contrast, are commonly employed to generate quantitative estimates for atmospheric O_2 levels through Earth's history. Estimates for Paleozoic pO_2 generated by GEOCARBSULF, one of the most widely implemented carbon and sulfur cycle models, have historically suggested high atmospheric O_2 level throughout the Paleozoic, in direct contradiction to competing models. In this study, we evaluate if GEOCARBSULF can predict relatively low Paleozoic O_2 levels. We first updated GEOCARBSULF by adopting the recent complication of the $\delta^{13}C$ value of marine buried carbonate and replacing the old formulation of sulfur isotope fractionation factor with the empirical sulfur isotope records. Afterwards, we constructed various O_2 evolution scenarios (with low O_2 levels in the early Paleozoic) and examined if GEOCARBSULF could reproduce these scenarios by varying the weathering/degassing fluxes of carbon and sulfur, or carbonate $\delta^{13}C$. We show that GEOCARBSULF can, in fact, maintain low-O_2 (even 1–5% atm) levels through the early Paleozoic by only varying the carbonate $\delta^{13}C$ within 2SD bounds permitted by the geological record. In addition, it can generate a middle–late Paleozoic rise in O_2 concentration, coincident with the diversification of land plants. However, given the complexity of the carbonate $\delta^{13}C$ record, we also argue that GEOCARBSULF cannot be used to track atmospheric O_2 levels until we have a better record of Paleozoic marine carbonate carbon isotope evolution.

INTRODUCTION

The protracted rise of atmospheric oxygen is one of the most obvious ways in which life has reshaped our planet. However, almost all aspects of the history of atmospheric oxygen have been fervently debated over the past few decades. For instance, there is still persistent debate about the role—if any—that land plants played in driving the rise of atmospheric oxygen over the Paleozoic (Bergman and others, 2004; Berner, 1987; Berner, 2001a; Berner, 2006b; Berner and Canfield, 1989; Lenton and others, 2016; Wallace and others, 2017). A series of geochemical redox proxies have been used to estimate the atmospheric O_2 levels qualitatively. Statistical analysis of iron speciation (Sperling and others, 2015) indicates widespread anoxic marine subsurface waters in the Cambrian. Cerium anomalies in well preserved marine cements and other marine precipitates confirmed that ocean anoxia was prevalent not only in the Cambrian but also through the Ordovician to Early Devonian (Wallace and others, 2017). The cerium anomaly record also argues for a continuous rise of surface O_2 levels through the Devonian, which has also been suggested using Mo isotope data (Dahl and others, 2010).

Although there are consistent advances in using geochemical paleo-redox proxies to predict O_2 levels qualitatively, quantitative estimates of atmospheric oxygen for the Phanerozoic still come from global biogeochemical models. Over geologic time scales (>1 million years), atmospheric O_2 levels are controlled by the carbon (C) and sulfur (S) sedimentary redox cycles (Berner, 1987). Oxidative weathering of organic carbon and pyrite (and oxidation of reduced gases) will consume O_2 while sediment burial of organic carbon and pyrite will release O_2.

The representative reactions for O_2 update are:

$$O_2 + CH_2O \rightarrow CO_2 + H_2O \tag{1}$$

$$15O_2 + 4FeS_2 + 8H_2O \rightarrow 2Fe_2O_3 + 8SO_4^{-2} + 16H^+ \tag{2}$$

The representative reactions for O_2 release are just the reverse of the reactions above. Based on these reactions, changes in atmospheric O_2 with time can be formulated as (Berner, 2004):

$$\frac{d[O_2]}{dt} = F_{bg} - F_{wg} - F_{mg} + \left(\frac{15}{8}\right)\left(F_{bp} - F_{wp} - F_{mp}\right) \quad (3)$$

Where F_{bg} and F_{bp} are the rate of burial of organic carbon and of pyrite sulfur in sediments respectively, F_{wg} and F_{wp} are the rate of oxidative weathering of organic carbon and of pyrite sulfur respectively, and F_{mg} and F_{mp} are the rate of oxidation of reduced carbon-containing gases and of reduced sulfur-containing gases released via diagenesis, metamorphism, and volcanism respectively. The embedded ratio refers to the stoichiometry of the reaction related to pyrite formation and oxidation.

Various numeric models have been built to estimate atmospheric O_2 levels over the Phanerozoic, and these models differ in how they calculate the weathering and burial fluxes of organic carbon and pyrite (Arvidson and others, 2013; Bergman and others, 2004; Berner, 2001b; Berner, 2006b; Berner and Canfield, 1989; Falkowski and others, 2005; Hansen and Wallmann, 2003; Lenton and others, 2016; Mills and others, 2014; Mills and others, 2016). The two mostly commonly utilized models for the Phanerozoic are GEOCARBSULF (Berner, 2006b; Berner, 2009) and COPSE (Bergman and others, 2004; Lenton and others, 2016; Mills and others, 2014). These models produce fundamentally different predictions for atmospheric oxygen levels over the Paleozoic. Specifically, GEOCARBSULF predicts near modern pO_2 throughout the Paleozoic (fig. 1), which implies that land plants were not essential to drive Earth to the high oxygen state characteristic of the modern world. COPSE, on the other hand, predicts low atmospheric oxygen throughout the early Paleozoic, and a rise towards modern levels during the middle-late Paleozoic coincident with the evolution of land plants (fig. 1).

These differences between models arise from the methods used to calculate O_2 fluxes: in the GEOCARBSULF model, carbon and sulfur burial rates are inverted from isotope mass balance, whereas the COPSE model calculates their burial rates based on assumed primary productivity and nutrient recycling. Primary productivity and nutrient recycling are difficult to estimate for Earth's past, especially when considering the Paleozoic where geologic data are sparse. In COPSE (Bergman and others, 2004), an increase of carbon burial on land in the Carboniferous was driven by doubling the C:P burial ratio of land organic matter to represent the effects of enhanced preservation in swamps and mires. This model

condition contributes to a mid-Paleozoic O_2 rise. Similarly, the assumption of a high C:P ratio and high land primary productivity starting from ~470 Ma leads to the rapid rise of O_2 in the early Paleozoic in the more recent version of COPSE (Lenton and others, 2016). Therefore, the COPSE model is parameterized in such a way as to directly drive a rise in atmospheric oxygen levels with the emergence of land plants, and thus does not provide truly independent support for the link between land plant evolution and global oxygenation.

Here we revisit GEOCARBSULF to explore if this model can be consistent with land plants reshaping our atmosphere. Specifically, we test whether atmospheric O_2 can be maintained at relatively low levels in the early Paleozoic, and if O_2 can rise over the latter half of the Paleozoic in GEOCARBSULF. We address this question by investigating the sources and sinks of O_2, as shown in equation (3). First, we conducted sensitivity analyses on the weathering and degassing of carbon and sulfur reservoir, which directly influences the O_2 sinks and also determines the O_2 sources indirectly through their control on the burial rate of organic carbon and pyrite. Second, we investigated the effect on O_2 levels of a single term — the $\delta^{13}C$ value of buried carbonate through time, which directly reflects the burial of organic carbon and in turn regulates the rates of O_2 release. In addition, we used a more reasonable value of the initial sulfate proportion in the crust and performed sensitivity analyses on $\delta^{13}C$ value of buried carbonate using this updated value. Building from this work we argue that GEOCARBSULF can produce low Paleozoic O_2 level by only varying the $\delta^{13}C$ values within uncertainties of the geological record. In other words, variation of $\delta^{13}C$ values of carbonate plays a big role in controlling the model output. Therefore, unless we have a better constrained and more robust carbonate carbon isotope record, GEOCARBSULF is not capable of pinpointing atmospheric O_2 evolution through Paleozoic.

A BRIEF INTRODUCTION TO GEOCARBSULF

GEOCARBSULF was constructed upon a series of seminal studies on global carbon and sulfur cycling. The numerical models for reconstructing the mass of oxidized and reduced carbon and sulfur

through the Phanerozoic build heavily upon the work of Garrels and Lerman (1981; 1984), which outlined the central tenets in global isotope mass balance modeling. Berner (1987) made a major modification when he put forward the idea of "rapid recycling" to provide strong negative feedback on O_2 fluctuations and predicted atmospheric O_2 evolution through the Phanerozoic. In rapid recycling, the mass of each sedimentary reservoir is divided into young (rapidly weathering) and old (slowly weathering) components. All newly buried carbon and sulfur go to the young reservoirs. In this way, whenever there is a rapid burial of organic carbon or pyrite (leading to rapid O_2 release), there will be a subsequent rapid weathering of those young organic carbon or pyrite (leading to rapid O_2 consumption), which will mitigate the fluctuation of O_2. To provide a stronger negative feedback, Berner and others (2000) and Berner (2001b) also incorporated O_2-dependent carbon and sulfur isotope fractionation into the model. In 2006, Berner combined GEOCARB III (a classic model to reconstruct the CO_2 levels in the past and largely developed by Berner) and the O_2 model into a single model called GEOCARBSULF, which could simultaneously calculate the evolution of CO_2 and O_2 through the Phanerozoic (Berner, 2006b). In the following years, GEOCARBSULF was continuously updated and refined (for example, inclusion of the weathering of volcanic rocks and reconsideration of the fractionation of carbon isotopes) (Berner, 2006a; Berner, 2009) and the most recent version is described by Royer and others (2014).

An overview of the geochemical cycles of carbon, sulfur and oxygen in GEOCARBSULF is presented in figure 2. The full equations and parameters of GEOCARBSULF are described in detail in the Appendix. Below we list the key equations (with parameters defined in figure 2 and the Appendix) in GEOCARBSULF that are used to calculate the fluxes related to O_2 evolution.

$$F_{wgy} = f_A \cdot f_R \cdot \mathrm{k_{wgy}} \cdot G_y(t) \tag{4}$$

$$F_{wga} = f_R \cdot F_{wga\_}0 \tag{5}$$

$$F_{wcy} = f_A \cdot f_D \cdot f_L \cdot f_E \cdot f_{Bb\_ca} \cdot k_{wcy} \cdot C_y(t) \tag{6}$$

$$F_{wca} = f_A \cdot f_D \cdot f_L \cdot f_E \cdot f_{Bb\_ca} \cdot F_{wca\_}0 \tag{7}$$

$$F_{wpy} = f_A \cdot f_R \cdot \mathrm{k_{wpy}} \cdot P_y(t) \tag{8}$$

$$F_{wpa} = f_R \cdot F_{wpa\_}0 \tag{9}$$

$$F_{wsy} = f_A \cdot f_D \cdot \mathrm{k_{wsy}} \cdot S_y(t) \tag{10}$$

$$F_{wsa} = f_A \cdot f_D \cdot F_{wsa\_}0 \tag{11}$$

$$F_{mg} = f_{SR} \cdot F_{mg\_}0 \tag{12}$$

$$F_{mc} = f_{SR} \cdot f_C \cdot F_{mc\_}0 \tag{13}$$

$$F_{mp} = f_{SR} \cdot F_{mp\_}0 \tag{14}$$

$$F_{ms} = f_{SR} \cdot F_{ms\_}0 \tag{15}$$

$$F_{bg} = \frac{1}{\Delta^{13}C} \times \left[(\delta^{13}\mathrm{C} - \mathrm{dlcy}) \cdot \mathrm{F_{wcy}} + (\delta^{13}\mathrm{C} - \mathrm{dlca}) * \mathrm{F_{wca}} + (\delta^{13}\mathrm{C} - \mathrm{dlgy}) * \mathrm{F_{wgy}} + (\delta^{13}\mathrm{C} - \mathrm{dlga}) * \mathrm{F_{wga}} + (\delta^{13}\mathrm{C} - \mathrm{dlca}) * \mathrm{F_{mc}} + (\delta^{13}\mathrm{C} - \mathrm{dlga}) * \mathrm{F_{mg}}\right] \tag{16}$$

$$F_{bp} = \frac{1}{\Delta^{34}S} \times \left[(\delta^{34}\mathrm{S} - \mathrm{dlsy}) \cdot \mathrm{F_{wsy}} + (\delta^{34}\mathrm{S} - \mathrm{dlsa}) * \mathrm{F_{wsa}} + (\delta^{34}\mathrm{S} - \mathrm{dlpy}) * \mathrm{F_{wpy}} + (\delta^{34}\mathrm{S} - \mathrm{dlpa}) * \mathrm{F_{wpa}} + (\delta^{34}\mathrm{S} - \mathrm{dlsa}) * \mathrm{F_{ms}} + (\delta^{34}\mathrm{S} - \mathrm{dlpa}) * \mathrm{F_{mp}}\right] \tag{17}$$

$$\frac{d[O_2]}{dt} = F_{bg} - F_{wgy} - F_{wga} - F_{mg} + \left(\frac{15}{8}\right)\left(F_{bp} - F_{wpy} - F_{wpa} - F_{mp}\right) \tag{18}$$

Using the "rapid recycling" concept, the weatherable shell is divided into a young reservoir (F_{wgy}, F_{wcy}, F_{wpy}, F_{wsy}) and an old reservoir (F_{wga}, F_{wca}, F_{wpa}, F_{wsa}). The isotope mass balance technique is given in equations (16) and (17). In addition to the terms defined above (and in the caption of figure 2), f_A is land area at time (t) relative to the present-day; f_D is global river runoff at time (t) relative to the present-day in the absence of changing CO_2 and solar luminosity; f_L is land area covered by carbonates at time (t) relative to the present-day; f_R is effect of relief on chemical weathering at time (t) relative to the present-day; f_{SR} is seafloor creation rate at time (t) relative to the present-day; f_E is effect of plants on weathering rate at time (t) relative to the present-day; f_{BB} is effect of CO_2 on plant-assisted weathering for carbonates at time (t) relative to the present-day; k_{wgy} is rate of mass dependence for young organic carbon

weathering; k_{wcy} is rate of mass dependence for young carbonate weathering; k_{wpy} is rate of mass dependence for young pyrite sulfur weathering; k_{wsy} is rate of mass dependence for young sulfate sulfur weathering; F_{wga}_0 is carbon flux from weathering of old sedimentary organic matter at present-day; F_{wca}_0 is carbon flux from weathering of old carbonates at present-day; F_{wpa}_0 is sulfur flux from weathering of old pyrite at present-day; F_{wsa}_0 is sulfur flux from weathering of old sulfate at present-day; F_{mg}_0 is carbon degassing flux of organic carbon at present-day; F_{mc}_0 is carbon degassing flux of carbonates at present-day; F_{mp}_0 is sulfur degassing flux of pyrite at present-day; F_{ms}_0 is sulfur degassing flux of sulfate at present-day; $\Delta^{13}C$ is the carbon isotope fractionation between carbonate and organic carbon; $\delta^{13}C$ is the isotope value of carbonate carbon; dlgy, dlga, dlcy and dlca are the $\delta^{13}C$ value of young organic carbon, old organic carbon, young carbonate carbon and old carbonate carbon respectively; $\Delta^{34}S$ is the carbon isotope fractionation between gypsum and pyrite; $\delta^{34}S$ is the isotope value of gypsum sulfur; dlpy, dlpa, dlsy and dlsa are the $\delta^{34}S$ value of young pyrite sulfur, old pyrite sulfur, young gypsum sulfur and old gypsum sulfur respectively.

MODIFICATION TO GEOCARBSULF

We modified the GEOCARBSULF version presented by Royer and others (2014), which is largely identical to the initial versions of GEOCARBSULF (Berner, 2006b; Berner, 2009). In GEOCARBSULF, the carbon and sulfur isotope fractionation ($\Delta^{13}C$ and $\Delta^{34}S$) is dependent on the O_2 levels, which could provide a negative feedback to the O_2 fluctuation and help avoid unrealistic atmospheric O_2 levels throughout the Phanerozoic. Their relationship can be formulated as follows:

$$\Delta^{13}\mathrm{C} = \Delta^{13}\mathrm{C\_0} + [J \cdot (RO_2 - 1)] \tag{19}$$

$$\Delta^{34}\mathrm{S} = \Delta^{34}\mathrm{S\_0} \times {RO_2}^{n} \tag{20}$$

Where $\Delta^{13}C$_0 represents the carbon isotopic fractionation between carbonate and organic matter at present-day; J is an adjustable curve fit parameter; RO_2 is the mass of oxygen in the atmosphere in the past relative to the present day; $\Delta^{34}S$_0 represents the sulfur isotopic fractionation between gypsum and pyrite at present-day; n is an adjustable fit parameter. Unlike the relationship between O_2 and the carbon

isotope fractionation factor ($\Delta^{13}C$), which is based on lab experiments (Beerling and others, 2002; Berner and others, 2000), the O_2 dependency of $\Delta^{34}S$ is not well constrained and the relationship used in GEOCARBSULF is likely overly simplified. Because the majority of pyrite formed through sulfate reduction will be reoxidized (and potentially processed by bacterial disproportionation), which could possibly produce bigger sulfur isotope fractionations (for example, Berner, 2001a; Canfield, 2001; Johnston, 2011), it is very difficult to constrain the sulfur isotope fractionation system only by experimental approach. Making things more complex, recent experimental studies (Sim and others, 2011) have shown that large sulfur isotope fractionations can be also obtained from sulfate reduction alone without the need for disproportionation.

To quantify $\Delta^{34}S$ through time, Wu and others (2010) adopted two methods: an arithmetic difference method ($\Delta^{34}S = \delta^{34}S_{sw} - \delta^{34}S_{py}$) which is totally based on geological empirical records, and an independent method that calls upon $\Delta^{33}S$ and sulfur cycle models. These two methods yield similar results (particularly before the Permian) and proves the robustness of using the empirical records to determine $\Delta^{34}S$. Although those geological records can only represent a small fraction of what was deposited, they do construct the current best available $\Delta^{34}S$ curve. Therefore, in our revised model calculations, we used an empirically based record of $\Delta^{34}S$ (and assign 4‰ as the 2SD), which eliminates the strong O_2 feedback in the sulfur cycle. We also updated GEOCARBSULF by replacing the old $\delta^{13}C$ curve with the new 10 million years average curve (Grossman and others, 2008; Saltzman and Thomas, 2012; Veizer and others, 1999). Similar to Royer and others (2014), we used a Monte Carlo approach (10000 resampling) to quantify the errors of the model outputs. During each resample, GEOCARBSULF can fail at a specific time step for several reasons: 1) Any carbon or sulfur flux goes negative; 2) Calculated CO_2 is less than 150 ppm or bigger than 50000 ppm; 3) Calculated CO_2 or O_2 at 0 Ma deviate from their measured values (CO_2 is not in the 200–300 ppm range and O_2 is not in the 19–23% range) (Royer and others, 2014). Following the above two updates, we ran GEOCARBSULF with a starting atmospheric O_2 level of 1% and 5% respectively at 570 Ma. We also run GEOCARBSULF with updated $\delta^{13}C$ curve but keeping the old $\Delta^{34}S$ formulation. Compared with the model run using the old $\Delta^{34}S$ formulation (fig. 3A), using

updated $\Delta^{34}S$ did not help lower O_2 level in the early Paleozoic (fig. 3B), but does serve to remove unrealistic negative feedback.

In addition to the updates related to the carbon and sulfur isotope system, essential to our new method (sensitivity tests) is that it allows us to input the desired model output (that is, O_2 evolution) and observe the underlying parameter changes required for the model to generate such an output. This is a modification of the traditional use of GEOCARBSULF where one predicts O_2 evolution from carbon and sulfur fluxes and isotope records. One set of underlying parameters that could be explored using this new method is the weathering and degassing fluxes of carbonates, organic carbon, sulfate and pyrite, which could affect the O_2 sink, as well as the O_2 source via isotope mass balance (equations 16 and 17). There are large uncertainties for these parameters in the current version of GEOCARBSULF. For example, the total land area that experienced extensive weathering, and the global runoff through time, are not well constrained (Royer and others, 2014). In addition, the oxygen dependency of the weathering rate of organic carbon and pyrite is debated (for example, Bolton and others, 2006; Lasaga and Ohmoto, 2002). The volcanic degassing rate, directly linked to degassing fluxes of carbon and sulfur, is likewise under continuous revision (for example, Berner, 2004; McKenzie and others, 2016; Van Der Meer and others, 2014). Another underlying parameter that has large uncertainties is the $\delta^{13}C$ of marine dissolved inorganic carbon (DIC), which is derived from buried carbonate and influences the calculated organic carbon burial rate — a key O_2 source. The record of burial carbonate $\delta^{13}C$ before the Mid-Jurassic is predominantly from measurements of platform carbonates, which exhibit greater spatial heterogeneity in $\delta^{13}C$ values than those from the Mid-Jurassic to Cenozoic measurements of pelagic carbonates (Panchuk and others, 2006; Saltzman and Thomas, 2012). Lastly, the initial reservoir sizes of sulfate and pyrite in the crust, which will shape Paleozoic redox conditions, are poorly constrained.

Here, we use the new method to test if GEOCARBSULF can maintain a low atmospheric O_2 level in the early Paleozoic given available empirical constraints. To do this, we first constructed four example pO_2 evolution scenarios through the Paleozoic (fig. 4), which are based on paleo-proxy records and previous model studies (fig. 1) and will be used as an input to our new methods in the following

sections. We used scenarios that cover a wide spectrum of delayed O_2 evolution patterns and thus can be used to test the potential for predicting these oxygenation histories using GEOCARBSULF.

SENSITIVITY TESTS OF THE WEATHERING AND DEGASSING FLUXES OF CARBON AND SULFUR ON O_2 LEVELS

We applied our new method to investigate the sensitivity of O_2 levels to the weathering and degassing fluxes of different rock reservoirs, namely carbonate weathering (F_{wcy} and F_{wca}), organic carbon weathering (F_{wgy} and F_{wga}), carbonate degassing (F_{mc}), organic carbon degassing (F_{mg}), sulfate weathering (F_{wsy} and F_{wsa}), sulfate degassing (F_{ms}), pyrite weathering (F_{wpy} and F_{wpa}), pyrite degassing (F_{mp}). We used a general-purpose optimization routine (L-BFGS-B in R language) to solve all the weathering and degassing fluxes of carbon and sulfur. Specifically, we multiply these fluxes each by a scaling factor, aiming to evaluate the relative importance of these fluxes in controlling pO_2. The modified equations are as follows (_S means scaling):

$$F_{wgy\_}S = S_{wg} \cdot f_A \cdot f_R \cdot \mathrm{k_{wgy}} \cdot G_y(t) \tag{21}$$

$$F_{wga\_}S = S_{wg} \cdot f_R \cdot F_{wga\_}0 \tag{22}$$

$$F_{wcy\_}S = S_{wc} \cdot f_A \cdot f_D \cdot f_L \cdot f_E \cdot f_{Bb\_ca} \cdot k_{wcy} \cdot C_y(t) \tag{23}$$

$$F_{wca\_}S = S_{wc} \cdot f_A \cdot f_D \cdot f_L \cdot f_E \cdot f_{Bb\_ca} \cdot F_{wca\_}0 \tag{24}$$

$$F_{wpy\_}S = S_{wp} \cdot f_A \cdot f_R \cdot \mathrm{k_{wpy}} \cdot P_y(t) \tag{25}$$

$$F_{wpa\_}S = S_{wp} \cdot f_R \cdot F_{wpa\_}0 \tag{26}$$

$$F_{wsy\_}S = S_{ws} \cdot f_A \cdot f_D \cdot \mathrm{k_{wsy}} \cdot S_y(t) \tag{27}$$

$$F_{wsa\_}S = S_{ws} \cdot f_A \cdot f_D \cdot F_{wsa\_}0 \tag{28}$$

$$F_{mg\_}S = S_{mg} \cdot f_{SR} \cdot F_{mg\_}0 \tag{29}$$

$$F_{mc\_}S = S_{mc} \cdot f_{SR} \cdot f_C \cdot F_{mc\_}0 \tag{30}$$

$$F_{mp\_}S = S_{mp} \cdot f_{SR} \cdot F_{mp\_}0 \tag{31}$$

$$F_{ms}\_S = S_{ms} \cdot f_{SR} \cdot F_{ms}\_0 \tag{32}$$

$$\begin{aligned} F_{bg}\_S = \frac{1}{\Delta^{13}C} \times \big[& (\delta^{13}\mathrm{C} - \mathrm{dlcy}) \cdot \mathrm{F_{wcy}}\_S + (\delta^{13}\mathrm{C} - \mathrm{dlca}) * \mathrm{F_{wca}}\_S + (\delta^{13}\mathrm{C} - \mathrm{dlgy}) \\ & * \mathrm{F_{wgy}}\_S + (\delta^{13}\mathrm{C} - \mathrm{dlga}) * \mathrm{F_{wga}}\_S + (\delta^{13}\mathrm{C} - \mathrm{dlca}) * \mathrm{F_{mc}}\_S \\ & + (\delta^{13}\mathrm{C} - \mathrm{dlga}) * \mathrm{F_{mg}}\_S \big] \end{aligned} \tag{33}$$

$$\begin{aligned} F_{bp}\_S = \frac{1}{\Delta^{34}S} \times \big[& (\delta^{34}\mathrm{S} - \mathrm{dlsy}) \cdot \mathrm{F_{wsy}}\_S + (\delta^{34}\mathrm{S} - \mathrm{dlsa}) * \mathrm{F_{wsa}}\_S + (\delta^{34}\mathrm{S} - \mathrm{dlpy}) \\ & * \mathrm{F_{wpy}}\_S + (\delta^{34}\mathrm{S} - \mathrm{dlpa}) * \mathrm{F_{wpa}}\_S + (\delta^{34}\mathrm{S} - \mathrm{dlsa}) * \mathrm{F_{ms}}\_S \\ & + (\delta^{34}\mathrm{S} - \mathrm{dlpa}) * \mathrm{F_{mp}}\_S \big] \end{aligned} \tag{34}$$

$$\begin{aligned} \frac{d[O_2]}{dt} = & F_{bg}\_S - F_{wgy}\_S - F_{wga}\_S - F_{mg}\_S \\ & + \left(\frac{15}{8}\right)\left(F_{bp}\_S - F_{wpy}\_S - F_{wpa}\_S - F_{mp}\_S\right) \end{aligned} \tag{35}$$

The method searches for the optimized value for each scaling factor (as close as to 1, meaning the new flux is as close as to the original flux) needed to match a predicted O_2 at each time step. Specifically, using equation (21) to (35), we could solve F_{ms}_S in terms of F_{wgy}_S, F_{wga}_S, F_{wcy}_S, F_{wca}_S, F_{wpy}_S, F_{wpa}_S, F_{wsy}_S, F_{wsa}_S, F_{ng}_S, F_{mc}_S, F_{mp}_S and $d[O_2]/dt$. Afterwards, we could use L-BFGS-B to minimize the following expression:

$$\begin{aligned} & \left|\frac{F_{wgy}\_S + F_{wga}\_S - F_{wgy} - F_{wga}}{F_{wgy} + F_{wga}}\right| + \left|\frac{F_{wcy}\_S + F_{wca}\_S - F_{wcy} - F_{wca}}{F_{wcy} + F_{wca}}\right| \\ & + \left|\frac{F_{wpy}\_S + F_{wpa}\_S - F_{wpy} - F_{wpa}}{F_{wpy} + F_{wpa}}\right| \\ & + \left|\frac{F_{wsy}\_S + F_{wsa}\_S - F_{wsy} - F_{wsa}}{F_{wsy} + F_{wsa}}\right| + \left|\frac{F_{mg}\_S - F_{mg}}{F_{mg}}\right| \\ & + \left|\frac{F_{mc}\_S - F_{mc}}{F_{mc}}\right| + \left|\frac{F_{mp}\_S - F_{mp}}{F_{mp}}\right| + \left|\frac{F_{ms}\_S - F_{ms}}{F_{ms}}\right| \end{aligned} \tag{36}$$

We assign a lower bound of 0 to the seven scaling factors (carbonate weathering, organic carbon weathering, carbonate degassing, organic carbon degassing, sulfate weathering, pyrite weathering and pyrite degassing) and assign no bound to the scaling factor of sulfate degassing (since this scaling factor is solved from the other seven scaling factors). The model runs from 570 to 300 Ma and fails at various time steps for different scenarios. In addition, some scaling factors are required to fluctuate significantly within a geologically short time interval, which is physically implausible. For example, with the carbonate weathering scaling factor (fig. 5B), extremely large fluctuations (for example, a drop from 1 to 0 in 20 million years during Ordovician for Scenario 3 and 4) are required.

SENSITIVITY TESTS OF CARBONATE $\delta^{13}C$ ON O_2 LEVELS

We argue that the most poorly constrained, yet impactful input parameter for GEOCARBSULF is the carbonate $\delta^{13}C$ values chosen for given time bin, which tightly controls the burial rate of organic carbon. Due to the complexity surrounding the empirical carbonate $\delta^{13}C$ records, the $\delta^{13}C$ of buried carbonate in the Paleozoic used in GEOCARBSULF may not be the true average $\delta^{13}C$ of the ocean (for example, Saltzman and Thomas, 2012), thus influencing the predicted O_2 level. As demonstrated in Royer and others (2014) and Mills and others (2016), the atmospheric O_2 predicted by isotope mass balance is highly sensitive to assumed carbonate $\delta^{13}C$. Assuming all the weathering and degassing fluxes of carbon and sulfur are the same with the fluxes in the original GEOCARBSULF (that is, all scaling factors are 1), it is straightforward to apply the new method to solve carbonate $\delta^{13}C$ for different O_2 scenarios. Since we only have 1 unknown parameter (carbonate $\delta^{13}C$), we could directly solve this parameter and its solution is as follows:

$$\delta^{13}\mathrm{C} = \frac{F_{bg} \cdot \Delta^{13}C + F_{wcy} \cdot \mathrm{dlcy} + F_{wca} \cdot \mathrm{dlca} + F_{wgy} \cdot \mathrm{dlgy} + F_{wga} \cdot \mathrm{dlga} + F_{mc} \cdot \mathrm{dlca} + F_{mg} \cdot \mathrm{dlga}}{F_{wcy} + F_{wca} + F_{wgy} + F_{wga} + F_{mc} + F_{mg}} \quad (37)$$

As shown in figure 6, the carbonate $\delta^{13}C$ required to fit each O_2 scenario is consistently within the range of $\delta^{13}C$ records through the Paleozoic, and almost always within 2SD of the long term running average. The overall evolving trends of the required $\delta^{13}C$ across all scenarios and the $\delta^{13}C$ record are

similar, and the CO_2 predicted is similar to that from the original GEOCARBSULF model (fig. 7). In all scenarios, the organic carbon burial rate increased through the Devonian (fig. 8A) and the pyrite burial rate decreased through the Paleozoic (fig. 8B).

Instead of calculating $\Delta^{13}C$ based on its relationship with O_2 levels, we could also derive $\Delta^{13}C$ through time from the geologic records (Hayes and others, 1999)), similar to what we did for $\Delta^{34}S$. We note that the compilation of Hayes and others (1999) may not represent the true global average $\Delta^{13}C$ because the $\delta^{13}C$ of organic carbon used to calculate $\Delta^{13}C$ is based solely on marine organic matter. Despite this, the required carbonate $\delta^{13}C$ values still fall into the range of the $\delta^{13}C$ record after this update (fig. 9B).

Besides carbonate $\delta^{13}C$, the initial sulfate proportion within the upper continental crust (50% of the total sulfur) at 570 Ma assumed in the original formulation GEOCARBSULF is considered unlikely based on several recent f_{py} estimates (for example, Canfield and Farquhar, 2009; Halevy and others, 2012) which argue for limited sulfate burial in the Precambrian and Early Cambrian. Therefore, as an initial attempt, we reduced the initial sulfate proportion in the crust from 50% to 20%, which is in qualitative agreement with the work of Canfield and Farquhar (2009). To maintain a realistic $\delta^{34}S$ value of the sulfate reservoirs after this proportion change, the $\delta^{34}S$ values of initial young and old pyrite in the original GEOCARBSULF are also adjusted (from -10‰ to 0‰). This change is not unreasonable, as the $\delta^{34}S$ of buried sedimentary pyrite was 5.7‰ at 570 Ma and was even higher than 5.7‰ in the Precambrian (Wu and others, 2010). Therefore, assigning 0‰ to the initial sedimentary pyrite is conservative. After these modifications, the required carbonate $\delta^{13}C$ is more enriched at each time step (fig. 10 vs fig. 6) but still fits reasonably well with the isotope records. The CO_2 predictions are again similar to the original GEOARBSULF (fig. 11).

DISCUSSION

Our sensitivity tests demonstrate that it is impossible to maintain a low atmospheric O_2 in the early Paleozoic followed by an O_2 rise to ~ 30% by the Late Carboniferous through varying only the

weathering and degassing fluxes of different rock reservoirs in GEOCARBSULF. Even over the short time interval where the model ran successfully and maintained consistent O_2 levels, some weathering and degassing rate variations were extreme, indicating inefficiency of these parameters in controlling atmospheric O_2. While these results confirm that inorganic weathering and degassing fluxes can alter the predictions drawn from carbon isotope mass balance (Shields and Mills, 2017), they also suggest that the dominant influence on O_2 variability over most of the Phanerozoic was not the weathering rates of organic carbon and pyrite but their burial rates (Berner, 2006b).

By removing the extreme negative feedback from the sulfur system and changing the input carbonate $\delta^{13}C$ within the geological data range, we can maintain a low O_2 level in GEOCARBSULF before the Devonian (or before the Silurian in the case of Scenario 4 — see fig. 4). This model output is in great contrast with that of Royer and others (2014), which could not produce low O_2 levels in the early Paleozoic. Compared with figure 3B, which also couldn't maintain a low O_2 level even after updating the $\delta^{13}C$ and $\Delta^{34}S$, our model outputs indicate that uncertainties in the variations in marine $\delta^{13}C$ is the biggest hurdle in predicting O_2. Our method also argues for a relative constant organic carbon burial rate through Ordovician and Silurian, and a continuous increase of organic carbon burial rate through Devonian (fig. 8A), which correlates with the diversification of vascular plants. Our predicted $\delta^{13}C$ is generally less variable than the observed record through this time (fig. 6 and 10). However, the empirical $\delta^{13}C$ of old platform carbonates, similar to modern shallow water carbonates, were likely influenced by many factors such as: diagenetic processes, mineralogical variability, vital effects caused by calcifying organisms, local water mass restriction, and carbon cycle perturbations (Brand and others, 2009; Mii and others, 1999; Panchuk and others, 2006; Saltzman and Thomas, 2012; Veizer and others, 1999). For example, the $\delta^{13}C$ of brachiopods exhibit substantial regional heterogeneity, with high values in the Russian Platform, low values in western North America, and intermediate values in the midcontinent (Grossman and others, 2008). Given this variability, the exact global curve of the carbonate $\delta^{13}C$ through the Paleozoic is poorly known. Our modeling approach serves as an indirect way to inspect the global average carbonate $\delta^{13}C$ and bears significance for promoting further research on this issue.

There are uncertainties in many of the parameters in GEOCARBSULF and it is possible that some key processes are entirely absent from the model (Royer and others, 2014). Also, as a critical O_2 source, we note that the organic carbon burial rate calculated using the isotope mass balance method needs to be further examined and compared with geological records. But we have shown here that high atmospheric oxygen in the Paleozoic is not a reliable output from GEOCARBSULF, and low levels of atmospheric oxygen are equally or even more reasonable. Specifically, low atmospheric oxygen levels are also likely when there is a low initial sulfate proportion in the crust (for example, 20%). Therefore, although it is difficult with the current carbon isotope record to accurately predict atmospheric oxygen levels, GEOCARBSULF modeling could be consistent with the idea that the Paleozoic was a time of low atmospheric oxygen, and that land plants drove a step change in surface oxygen levels. A renewed effort to track carbon isotope gradients (following on Holmden and others, 1998) and careful screening of samples for diagenetic alteration are essential to build a better global $\delta^{13}C$ trend in Paleozoic, which could contribute to a tighter constraint on the O_2 evolution using GEOCARBSULF.

CONCLUSIONS

We show that by altering the carbonate $\delta^{13}C$ within permissible bounds, as well as revising the sulfate/sulfide ratio of the upper crust at the Precambrian-Cambrian boundary, GEOCARBSULF is consistent with the idea that the early Paleozoic was a time of low atmospheric oxygen, and that land plants drove a step change in surface oxygen levels. However, given the complexity of the carbonate $\delta^{13}C$ record, we also argue that GEOCARBSULF could not be used to pinpoint atmospheric O_2 levels until we have a more robust global $\delta^{13}C$ record in Paleozoic.

ACKNOWLEDGEMENTS

We thank Ellen Thomas for the carbonate $\delta^{13}C$ data. We thank Pincelli M. Hull for helpful discussions. Noah J. Planavsky acknowledges funding from the Alternative Earths NASA Astrobiology Institute and the Packard Foundation. Alexander J. Krause is funded by a UK NERC studentship. Edward W. Bolton acknowledges support from the Virtual Planetary Laboratory (Lead PI, Victoria Meadows, University of Washington). Benjamin J. W. Mills is funded by a University of Leeds Academic Fellowship. We thank Lee Kump and two anonymous reviewers for their inputs in improving the manuscript.

REFERENCES

Arvidson, R. S., Mackenzie, F. T., and Guidry, M. W., 2013, Geologic history of seawater: A MAGic approach to carbon chemistry and ocean ventilation: Chemical Geology, v. 362, p. 287–304.

Beerling, D. J., Lake, J. A., Berner, R. A., Hickey, L. J., Taylor, D. W., and Royer, D. L., 2002, Carbon isotope evidence implying high O2/CO2 ratios in the Permo-Carboniferous atmosphere: Geochimica et Cosmochimica Acta, v. 66, p. 3757–3767.

Bergman, N. M., Lenton, T. M., and Watson, A. J., 2004, COPSE: A new model of biogeochemical cycling over Phanerozoic time: American Journal of Science, v. 304, p. 397–437.

Berner, R. A., 1987, Models for carbon and sulfur cycles and atmospheric oxygen; application to Paleozoic geologic history: American Journal of Science, v. 287, p. 177–196.

Berner, R. A., 2001a, Modeling atmospheric O2 over Phanerozoic time: Geochimica et Cosmochimica Acta, v. 65, p. 685–694.

Berner, R. A., 2001b, Modeling atmospheric O2 over Phanerozoic time: Geochimica et Cosmochimica Acta, v. 65, p. 685–694.

Berner, R. A., 2004, The Phanerozoic Carbon Cycle: CO_2 and O_2: Oxford University Press, 158 p.

Berner, R. A., 2006a, Inclusion of the Weathering of Volcanic Rocks in the GEOCARBSULF Model: American Journal of Science, v. 306, p. 295–302.

Berner, R. A., 2006b, GEOCARBSULF: A combined model for Phanerozoic atmospheric O2 and CO2: Geochimica et Cosmochimica Acta, v. 70, p. 5653–5664.

Berner, R. A., 2009, Phanerozoic atmospheric oxygen: New results using the GEOCARBSULF model: American Journal of Science, v. 309, p. 603–606.

Berner, R. A., and Canfield, D. E., 1989, A new model for atmospheric oxygen over Phanerozoic time: American Journal of Science, v. 289, p. 333–361.

Berner, R. A., Petsch, S. T., Lake, J. A., Beerling, D. J., Popp, B. N., Lane, R. S., Laws, E. A., Westley, M. B., Cassar, N., Woodward, F. I., and Quick, W. P., 2000, Isotope Fractionation and Atmospheric Oxygen: Implications for Phanerozoic O2 Evolution: Science, v. 287, p. 1630–1633.

Bolton, E. W., Berner, R. A., and Petsch, S. T., 2006, The Weathering of Sedimentary Organic Matter as a Control on Atmospheric O2: II. Theoretical Modeling: American Journal of Science, v. 306, p. 575–615.

Brand, U., Tazawa, J., Sano, H., Azmy, K., and Lee, X., 2009, Is mid-late Paleozoic ocean-water chemistry coupled with epeiric seawater isotope records? Geology, v. 37, p. 823–826.

Canfield, D. E., 1998, A new model for Proterozoic ocean chemistry: Nature, v. 396, p. 450–453.

Canfield, D. E., 2001, Biogeochemistry of Sulfur Isotopes: Reviews in Mineralogy and Geochemistry, v. 43, p. 607–636.

Canfield, D. E., and Farquhar, J., 2009, Animal evolution, bioturbation, and the sulfate concentration of the oceans: Proceedings of the National Academy of Sciences, v. 106, p. 8123–8127.

Dahl, T. W., Hammarlund, E. U., Anbar, A. D., Bond, D. P. G., Gill, B. C., Gordon, G. W., Knoll, A. H., Nielsen, A. T., Schovsbo, N. H., and Canfield, D. E., 2010, Devonian rise in atmospheric oxygen correlated to the radiations of terrestrial plants and large predatory fish: Proceedings of the National Academy of Sciences, v. 107, p. 17911–17915.

Falkowski, P. G., Katz, M. E., Milligan, A. J., Fennel, K., Cramer, B. S., Aubry, M. P., Berner, R. A., Novacek, M. J., and Zapol, W. M., 2005, The Rise of Oxygen over the past 205 Million Years and the Evolution of Large Placental Mammals: Science, v. 309, p. 2202–2204.

Garrels, R. M., and Lerman, A., 1981, Phanerozoic cycles of sedimentary carbon and sulfur: Proceedings of the National Academy of Sciences, v. 78, p. 4652–4656.

Garrels, R. M., and Lerman, A., 1984, Coupling of the sedimentary sulfur and carbon cycles; an improved model: American Journal of Science, v. 284, p. 989–1007.

Glasspool, I. J., Scott, A. C., Waltham, D., Pronina, N., and Shao, L., 2015, The impact of fire on the Late Paleozoic Earth system: Frontiers in Plant Science, v. 6.

Grossman, E. L., Yancey, T. E., Jones, T. E., Bruckschen, P., Chuvashov, B., Mazzullo, S. J., and Mii, H., 2008, Glaciation, aridification, and carbon sequestration in the Permo-Carboniferous: The isotopic record from low latitudes: Palaeogeography, Palaeoclimatology, Palaeoecology, v. 268, p. 222–233.

Halevy, I., Peters, S. E., and Fischer, W. W., 2012, Sulfate Burial Constraints on the Phanerozoic Sulfur Cycle: Science, v. 337, p. 331–334.

Hansen, K. W., and Wallmann, K., 2003, Cretaceous and Cenozoic evolution of seawater composition, atmospheric O2 and CO2: A model perspective: American Journal of Science, v. 303, p. 94–148.

Hayes, J. M., Strauss, H., and Kaufman, A. J., 1999, The abundance of ^{13}C in marine organic matter and isotopic fractionation in the global biogeochemical cycle of carbon during the past 800 Ma: Chemical Geology, v. 161, p. 103–125.

Holmden, C., Creaser, R. A., Muehlenbachs, K., Leslie, S. A., and Bergström, S. M., 1998, Isotopic evidence for geochemical decoupling between ancient epeiric seas and bordering oceans: Implications for secular curves: Geology, v. 26, p. 567–570.

Johnston, D. T., 2011, Multiple sulfur isotopes and the evolution of Earth's surface sulfur cycle: Earth-Science Reviews, v. 106, p. 161–183.

Lasaga, A. C., and Ohmoto, H., 2002, The oxygen geochemical cycle: dynamics and stability: Geochimica et Cosmochimica Acta, v. 66, p. 361–381.

Lenton, T. M., Dahl, T. W., Daines, S. J., Mills, B. J. W., Ozaki, K., Saltzman, M. R., and Porada, P., 2016, Earliest land plants created modern levels of atmospheric oxygen: Proceedings of the National Academy of Sciences, v. 113, p. 9704–9709.

McKenzie, N. R., Horton, B. K., Loomis, S. E., Stockli, D. F., Planavsky, N. J., and Lee, C.-T. A., 2016, Continental arc volcanism as the principal driver of icehouse-greenhouse variability: Science, v. 352, p. 444–447.

Mii, H., Grossman, E. L., and Yancey, T. E., 1999, Carboniferous isotope stratigraphies of North America: Implications for Carboniferous paleoceanography and Mississippian glaciation: Geological Society of America Bulletin, v. 111, p. 960–973.

Mills, B. J. W., Belcher, C. M., Lenton, T. M., and Newton, R. J., 2016, A modeling case for high atmospheric oxygen concentrations during the Mesozoic and Cenozoic: Geology, p. G38231.1.

Mills, B., Daines, S. J., and Lenton, T. M., 2014, Changing tectonic controls on the long-term carbon cycle from Mesozoic to present: Geochemistry, Geophysics, Geosystems, v. 15, p. 4866–4884.

Panchuk, K. M., Holmden, C. E., and Leslie, S. A., 2006, Local Controls on Carbon Cycling in the Ordovician Midcontinent Region of North America, with Implications for Carbon Isotope Secular Curves: Journal of Sedimentary Research, v. 76, p. 200–211.

Royer, D. L., Donnadieu, Y., Park, J., Kowalczyk, J., and Goddéris, Y., 2014, Error analysis of CO2 and O2 estimates from the long-term geochemical model GEOCARBSULF: American Journal of Science, v. 314, p. 1259–1283.

Saltzman, M. R., and Thomas, E., 2012, Chapter 11 - Carbon Isotope Stratigraphy, in The Geologic Time Scale: Elsevier, Boston, p. 207–232.

Shields, G. A., and Mills, B. J. W., 2017, Tectonic controls on the long-term carbon isotope mass balance: Proceedings of the National Academy of Sciences, v. 114, p. 4318–4323.

Sim, M. S., Bosak, T., and Ono, S., 2011, Large Sulfur Isotope Fractionation Does Not Require Disproportionation: Science, v. 333, p. 74–77.

Sperling, E. A., Wolock, C. J., Morgan, A. S., Gill, B. C., Kunzmann, M., Halverson, G. P., Macdonald, F. A., Knoll, A. H., and Johnston, D. T., 2015, Statistical analysis of iron geochemical data suggests limited late Proterozoic oxygenation: Nature, v. 523, p. 451–454.

Van Der Meer, D. G., Zeebe, R. E., Hinsbergen, D. J. J. van, Sluijs, A., Spakman, W., and Torsvik, T. H., 2014, Plate tectonic controls on atmospheric CO2 levels since the Triassic: Proceedings of the National Academy of Sciences, v. 111, p. 4380–4385.

Veizer, J., Ala, D., Azmy, K., Bruckschen, P., Buhl, D., Bruhn, F., Carden, G. A. F., Diener, A., Ebneth, S., Godderis, Y., Jasper, T., Korte, C., Pawellek, F., Podlaha, O. G., and others, 1999, 87Sr/86Sr, δ13C and δ18O evolution of Phanerozoic seawater: Chemical Geology, v. 161, p. 59–88.

Wallace, M. W., Hood, A. vS., Shuster, A., Greig, A., Planavsky, N. J., and Reed, C. P., 2017, Oxygenation history of the Neoproterozoic to early Phanerozoic and the rise of land plants: Earth and Planetary Science Letters, v. 466, p. 12–19.

Watson, A., Lovelock, J. E., and Margulis, L., 1978, Methanogenesis, fires and the regulation of atmospheric oxygen: Biosystems, v. 10, p. 293–298.

Wildman, R. A., Hickey, L. J., Dickinson, M. B., Berner, R. A., Robinson, J. M., Dietrich, M., Essenhigh, R. H., and Wildman, C. B., 2004, Burning of forest materials under late Paleozoic high atmospheric oxygen levels: Geology, v. 32, p. 457–460.

Wu, N., Farquhar, J., Strauss, H., Kim, S.-T., and Canfield, D. E., 2010, Evaluating the S-isotope fractionation associated with Phanerozoic pyrite burial: Geochimica et Cosmochimica Acta, v. 74, p. 2053–2071.

FIGURE CAPTIONS

Fig. 1. Long-term carbon, sulfur, and oxygen cycles in GEOCARBSULF. Carbon cycle consists of fluxes between carbon in the surficial system including atmosphere, ocean, biosphere and soil (**C**), young organic carbon ($\mathbf{G_y}$), old organic carbon ($\mathbf{G_a}$), young carbonate ($\mathbf{C_y}$) and old carbonate ($\mathbf{C_a}$). Specifically, these fluxes are organic carbon burial ($\mathbf{F_{bg}}$), oxidative weathering of young organic carbon ($\mathbf{F_{wgy}}$) and old organic carbon ($\mathbf{F_{wga}}$), degassing of organic carbon from volcanism, metamorphism and diagenesis ($\mathbf{F_{mg}}$), organic carbon transfer from young to old reservoir ($\mathbf{F_{yog}}$), carbonate burial ($\mathbf{F_{bc}}$), weathering of young carbonate ($\mathbf{F_{wcy}}$) and old carbonate ($\mathbf{F_{wca}}$), degassing of carbonate from volcanism, metamorphism and diagenesis ($\mathbf{F_{mc}}$), and carbonate transfer from young to old reservoir ($\mathbf{F_{yoc}}$). Sulfur cycle consists of fluxes between sulfur in the surficial system including atmosphere, ocean, biosphere and soil (**S**), young pyrite

sulfur (**P_y**), old pyrite sulfur (**P_a**), young gypsum sulfur (**G_y**) and old gypsum sulfur (**G_a**). Specifically, these fluxes include pyrite burial (**F_{bp}**), oxidative weathering of young pyrite (**F_{wpy}**) and old pyrite (**F_{wpa}**), degassing of pyrite from volcanism, metamorphism and diagenesis (**F_{mp}**), pyrite transfer from young to old reservoir (**F_{yop}**), gypsum burial (**F_{bs}**), weathering of young gypsum (**F_{wsy}**) and old gypsum (**F_{wsa}**), degassing of gypsum from volcanism, metamorphism and diagenesis (**F_{ms}**), and gypsum transfer from young to old reservoir (**F_{yos}**). As shown in Equation (1), the sources of atmospheric O_2 are **F_{bg}** and **F_{bp}** (represented by the red arrow). The sinks are **F_{wgy}**, **F_{wga}**, **F_{mg}**, **F_{wpy}**, **F_{wpa}** and **F_{mp}** (represented by the blue arrow).

Fig. 2. O_2 evolution patterns through the Paleozoic. The red curve represents the O_2 prediction from the GEOCARBSULF model (Royer and others, 2014). The purple curve represents the O_2 prediction from the baseline COPSE model (Bergman and others, 2004). The red line shows the approximate maximum atmospheric O_2 level based on water column redox data (Canfield, 1998; Sperling and others, 2015). The blue line is the approximate O_2 maximum, based on burning experiments and wildfire feedbacks (Glasspool and others, 2015; Watson and others, 1978), but geochemical mass balance studies suggest pO_2 levels as high as 35% may be permissible (Wildman and others, 2004). The brown shaded area represents the trend of atmospheric O_2 evolution based on Mo isotopes (Dahl and others, 2010) and cerium anomaly records (Wallace and others, 2017).

Fig. 3. Predicted O_2 evolution from the GEOCARBSULF model with an initial O_2 level of 1% and 5%. (A) $\Delta^{34}S$ is derived from the old formulation (O_2 dependency) in GEOCARBSULF. (B) $\Delta^{34}S$ is derived from the geological records (Wu and others, 2010). The green line represents the predicted average O_2 level staring from 1% at 570 Ma and the red line represents the predicted average O_2 level staring from 5% at 570 Ma. The shaded area represents the average value ± 1SD.

Fig. 4. Atmospheric O_2 evolution scenarios through the Paleozoic constructed in this study. Scenario 1 and 2 try to simulate the O_2 level predicted by the cerium anomaly (Wallace and others, 2017). They keep O_2 at a low level (1% and 5% respectively) from the Early Cambrian to the Late Silurian and then force O_2 to rise to ~30% by the Late Carboniferous. Scenario 3 is atmospheric O_2 evolution after the baseline COPSE model (Bergman and others, 2004). Scenario 4 is a combination of atmospheric O_2 prediction after the baseline model and the updated COPSE model which integrates early plant colonization, biotic effects on silicate weathering and 25% increase in P weathering (Lenton and others, 2016).

Fig. 5. The scaling factors for various weathering fluxes required to reproduce different O_2 scenarios. (A) Scaling factor for organic carbon weathering rate. (B) Scaling factor for carbonate weathering rate. (C) Scaling factor for pyrite weathering rate. (D) Scaling factor for sulfate weathering rate. The shaded pink area represents the average value ± 2SD for Scenario 2. The error range for other scenarios is similar to that of Scenario 2. Different scenarios are described in figure 4.

Fig. 6. Carbonate $\delta^{13}C$ required to reproduce the four oxygen scenarios through the Paleozoic, and how they correlate with geologic record. The grey dots are the carbonate $\delta^{13}C$ compilation from Saltzman and Thomas (2012). The green dots are the $\delta^{13}C$ of brachiopod shells from Veizer (1999). The orange dots are the $\delta^{13}C$ of brachiopod shells compiled by Grossman and others (2008). The black line represents the moving average (10 Myrs) of all the carbonate $\delta^{13}C$ records. The brown area represents the average value ± 2SD. The shaded pink area represents the average value ± 2SD for Scenario 2. The error range for other scenarios is similar to that of Scenario 2. Different scenarios are described in figure 4.

Fig. 7. Atmospheric CO_2 predicted in the sensitivity tests of carbonate $\delta^{13}C$ for different scenarios, compared with the CO_2 prediction from the original GEOCARBSULF (Royer and others, 2014). Different scenarios are described in figure 4.

Fig. 8. Organic carbon and pyrite sulfur burial rate predicted in the sensitivity tests of carbonate $\delta^{13}C$ for different scenarios. (A) Organic carbon burial rate. (B) Pyrite sulfur burial rate. Notice that the pyrite burial rates for different scenarios are the same. Different scenarios are described in figure 4.

Fig. 9. $\Delta^{13}C$ from geological records and carbonate $\delta^{13}C$ required to reproduce the four oxygen scenarios using this $\Delta^{13}C$. (A) $\Delta^{13}C$ derived from Hayes and others (1999) through the Paleozoic. (B) Carbonate $\delta^{13}C$ required to reproduce the four oxygen scenarios using $\Delta^{13}C$ derived from geological records. The symbols are described in figure 6. Different scenarios are described in figure 4.

Fig. 10. Carbonate $\delta^{13}C$ required to reproduce the four oxygen scenarios through the Paleozoic, assuming 20% initial sulfate in the curst, and how they correlate with geologic record. The symbols are described in figure 6. Different scenarios are described in figure 4.

Fig. 11. Atmospheric CO_2 predicted in the sensitivity tests of carbonate $\delta^{13}C$ for different scenarios assuming 20% initial sulfate in the crust, compared with the CO_2 prediction from the original GEOCARBSULF (Royer and others, 2014). Different scenarios are described in figure 4.

Fig. 1

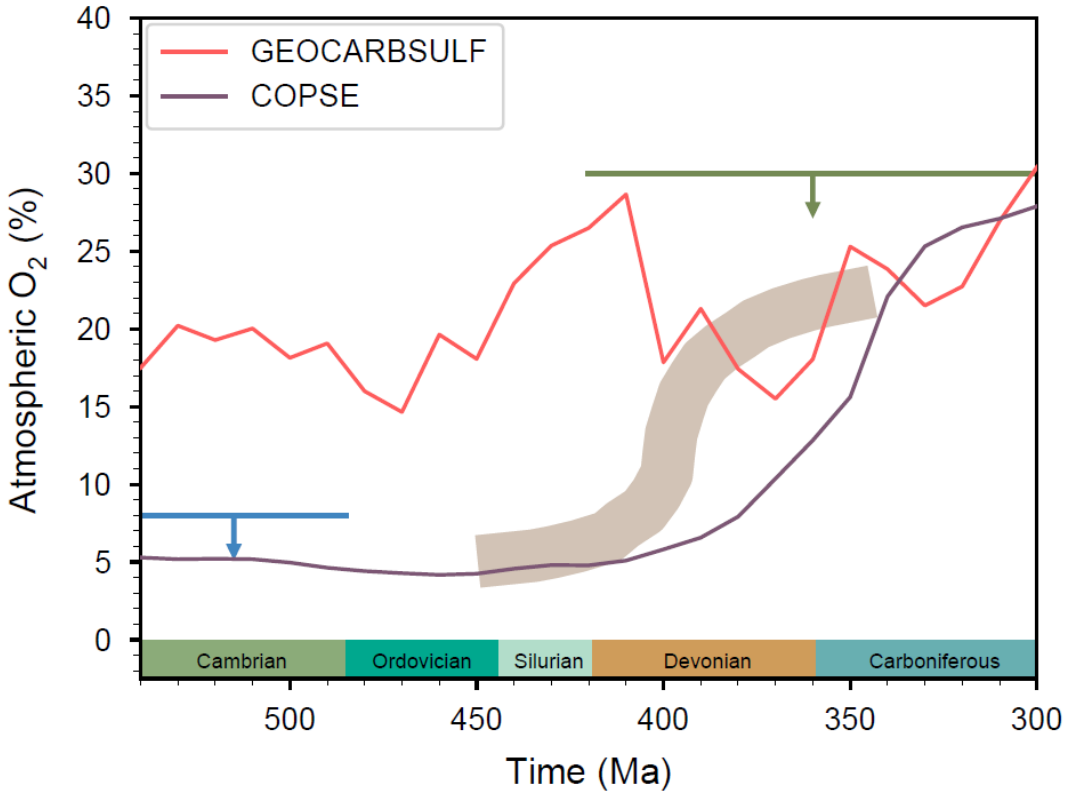
GEOCARBSULF
COPSE
Atmospheric O_2 (%)
40
35
30
25
20
15
10
5
0
Cambrian
Ordovician
Silurian
Devonian
Carboniferous
500
450
400
350
300
Time (Ma)

555

Fig. 2

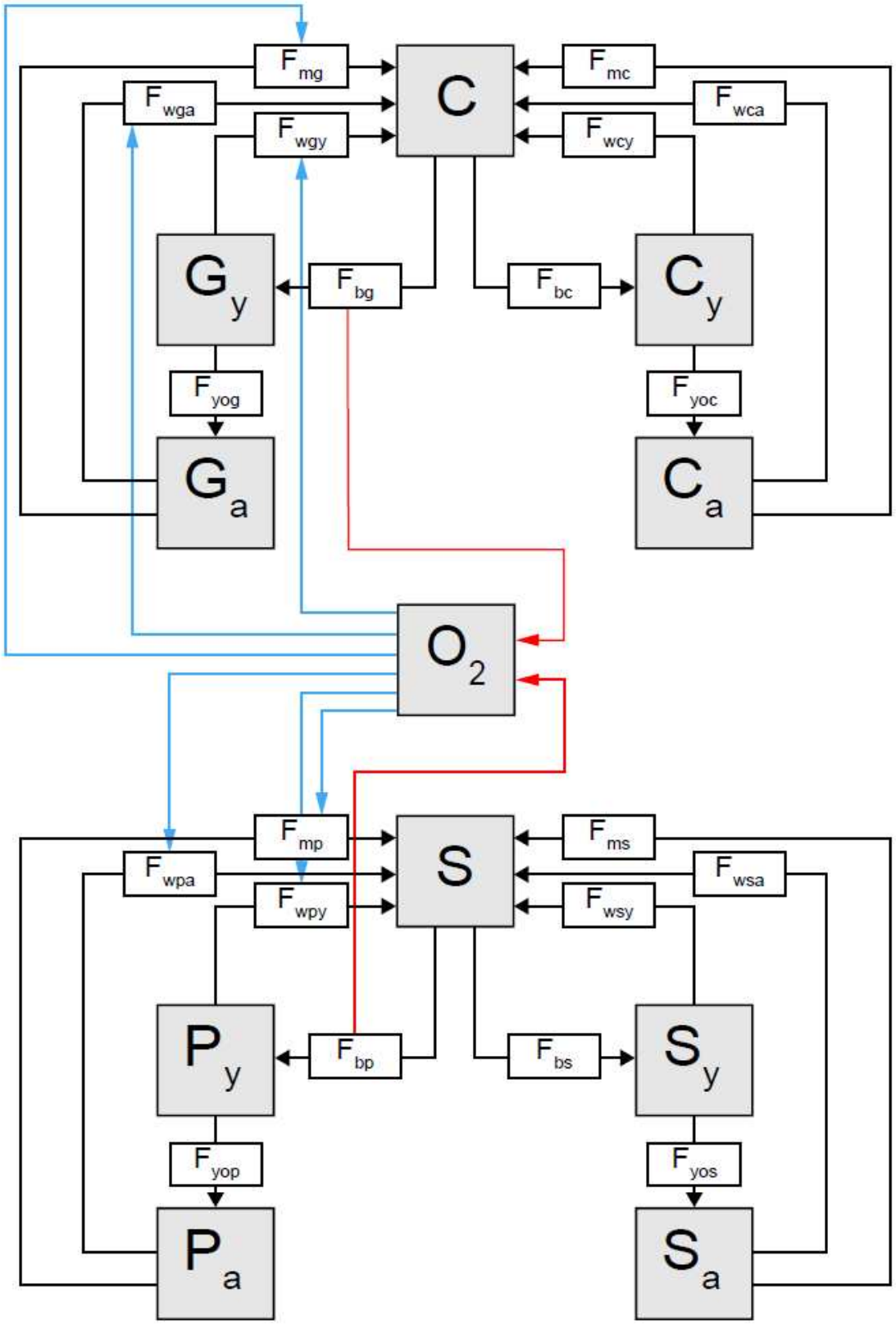
C
F mg
F mc
F wga
F wca
F wgy
F wcy
G y
C y
F bg
F bc
F yog
F yoc
G a
C a
O 2
S
F mp
F ms
F wpa
F wsa
F wpy
F wsy
P y
S y
F bp
F bs
F yop
F yos
P a
S a

556

Fig. 3

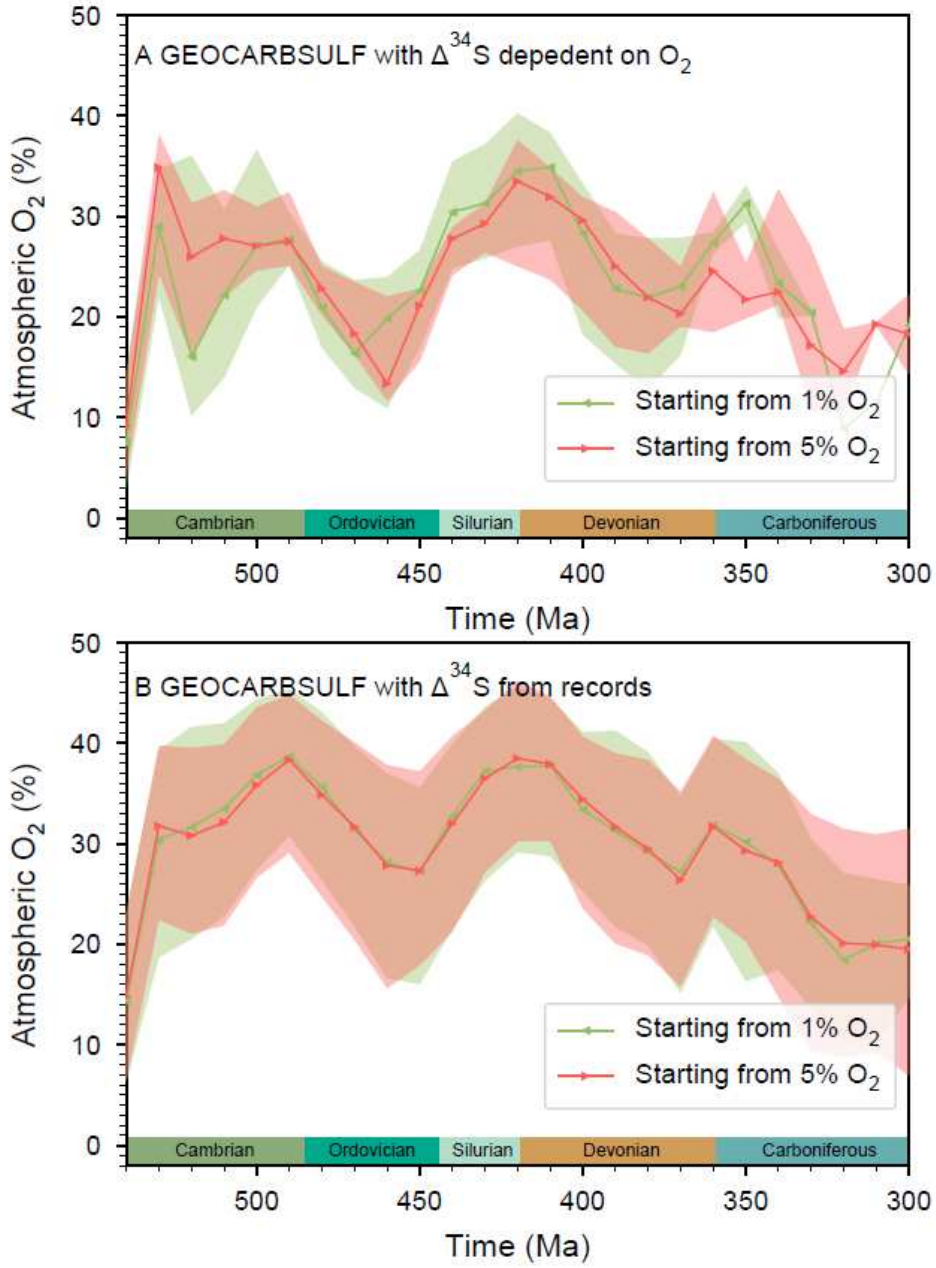
A GEOCARBSULF with Δ34S depedent on O2
Atmospheric O2 (%)
Starting from 1% O2
Starting from 5% O2
Cambrian
Ordovician
Silurian
Devonian
Carboniferous
Time (Ma)
B GEOCARBSULF with Δ34S from records
Atmospheric O2 (%)
Starting from 1% O2
Starting from 5% O2
Cambrian
Ordovician
Silurian
Devonian
Carboniferous
Time (Ma)

Fig. 4

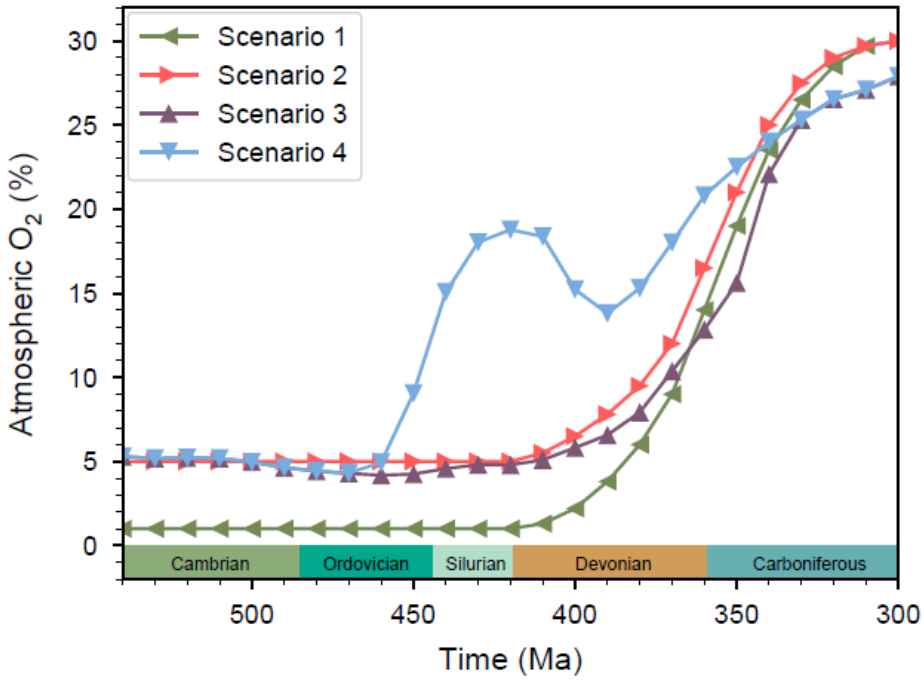
Scenario 1
Scenario 2
Scenario 3
Scenario 4
Atmospheric O_2 (%)
Time (Ma)
Cambrian
Ordovician
Silurian
Devonian
Carboniferous

Fig. 5

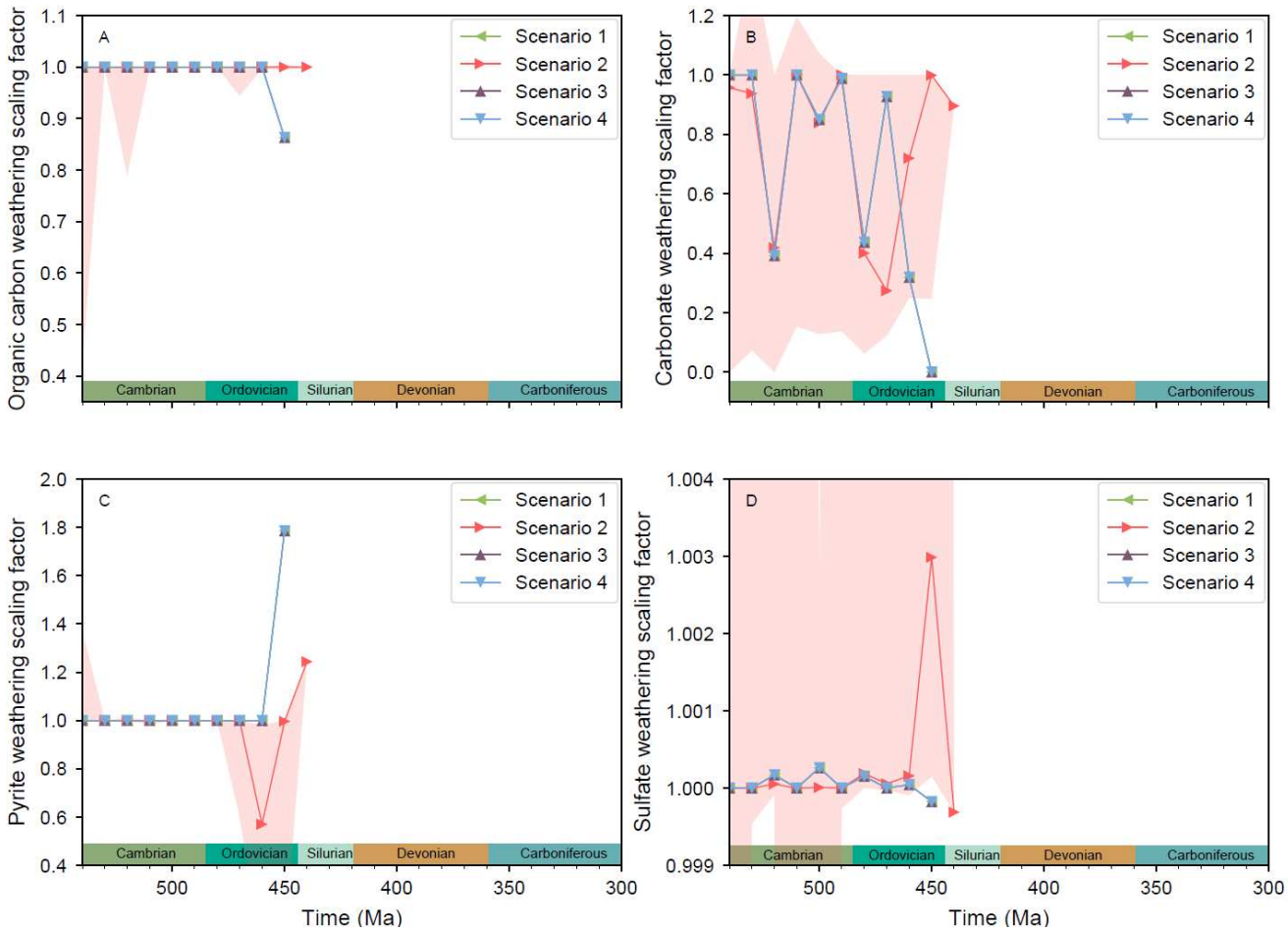
A
B
C
D
Scenario 1
Scenario 2
Scenario 3
Scenario 4
Organic carbon weathering scaling factor
Carbonate weathering scaling factor
Pyrite weathering scaling factor
Sulfate weathering scaling factor
Time (Ma)
Cambrian
Ordovician
Silurian
Devonian
Carboniferous

Fig. 6

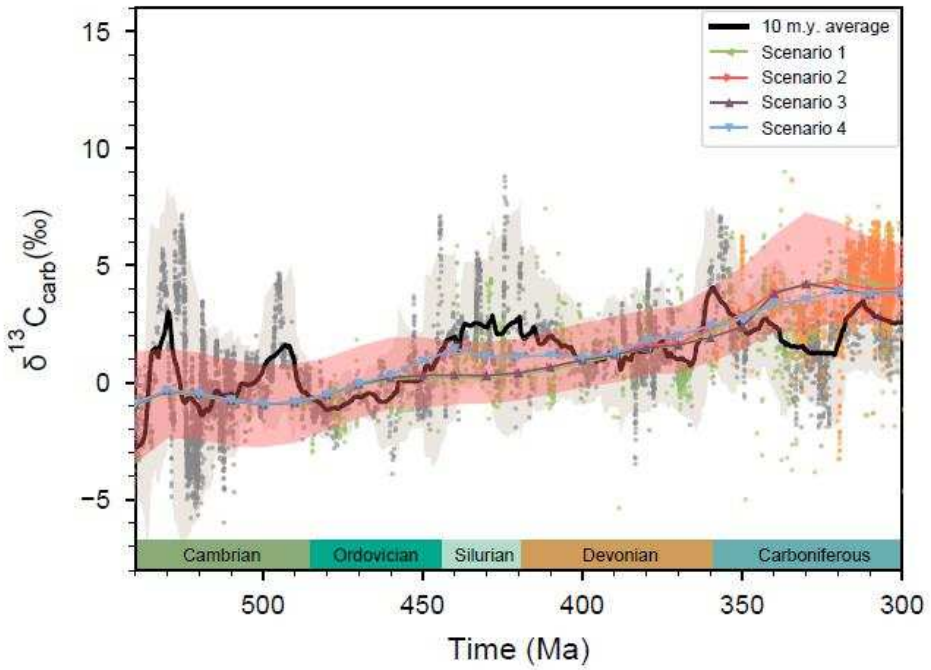
10 m.y. average
Scenario 1
Scenario 2
Scenario 3
Scenario 4
15
10
5
0
−5
δ13Ccarb(‰)
Cambrian
Ordovician
Silurian
Devonian
Carboniferous
500
450
400
350
300
Time (Ma)

Fig. 7

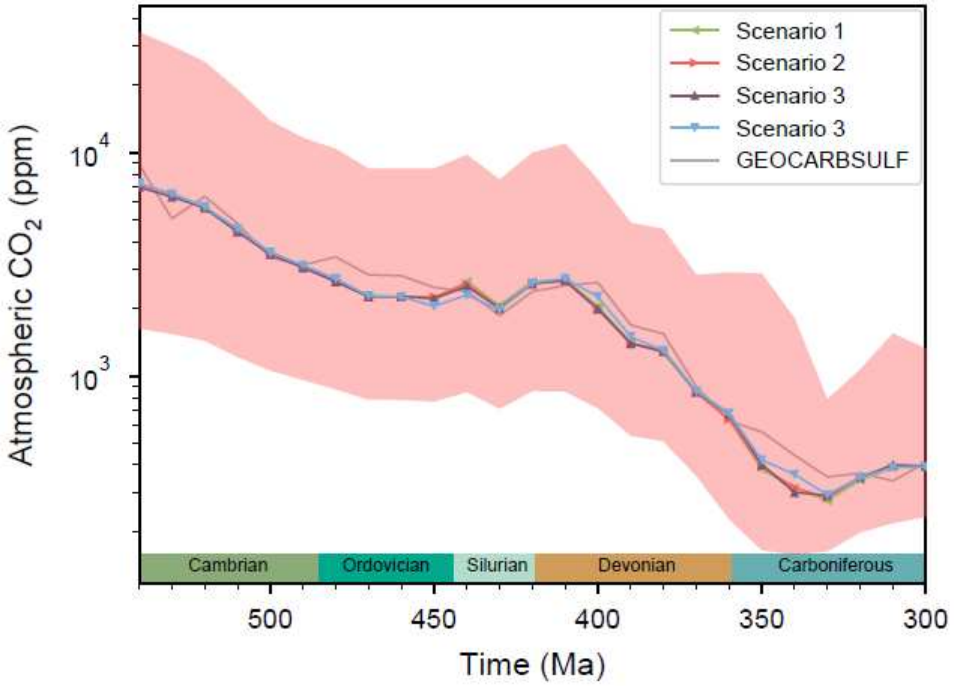
Scenario 1
Scenario 2
Scenario 3
Scenario 3
GEOCARBSULF
10^4
10^3
Atmospheric CO2 (ppm)
Cambrian
Ordovician
Silurian
Devonian
Carboniferous
500
450
400
350
300
Time (Ma)

Fig. 8

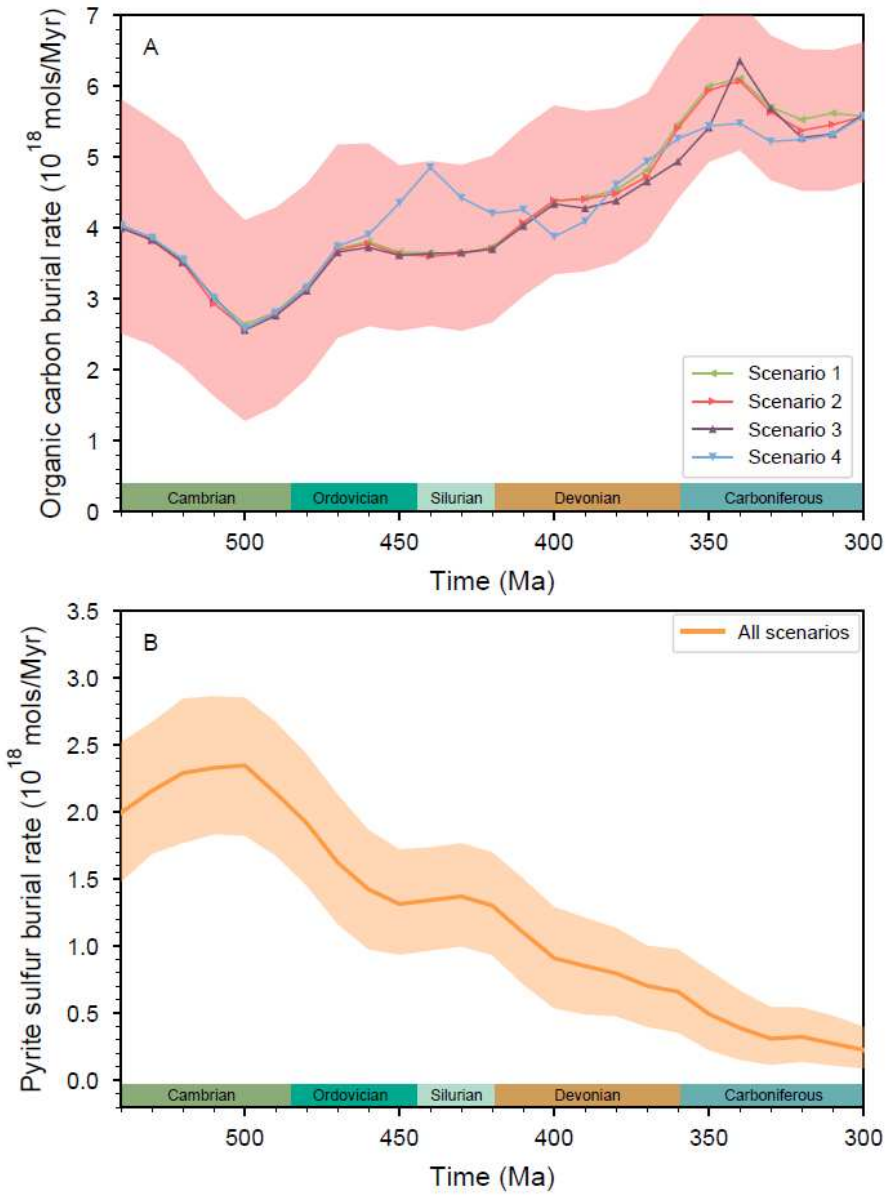
A
Organic carbon burial rate (10^{18} mols/Myr)
Scenario 1
Scenario 2
Scenario 3
Scenario 4
Cambrian
Ordovician
Silurian
Devonian
Carboniferous
Time (Ma)
B
Pyrite sulfur burial rate (10^{18} mols/Myr)
All scenarios
Cambrian
Ordovician
Silurian
Devonian
Carboniferous
Time (Ma)

Fig. 9

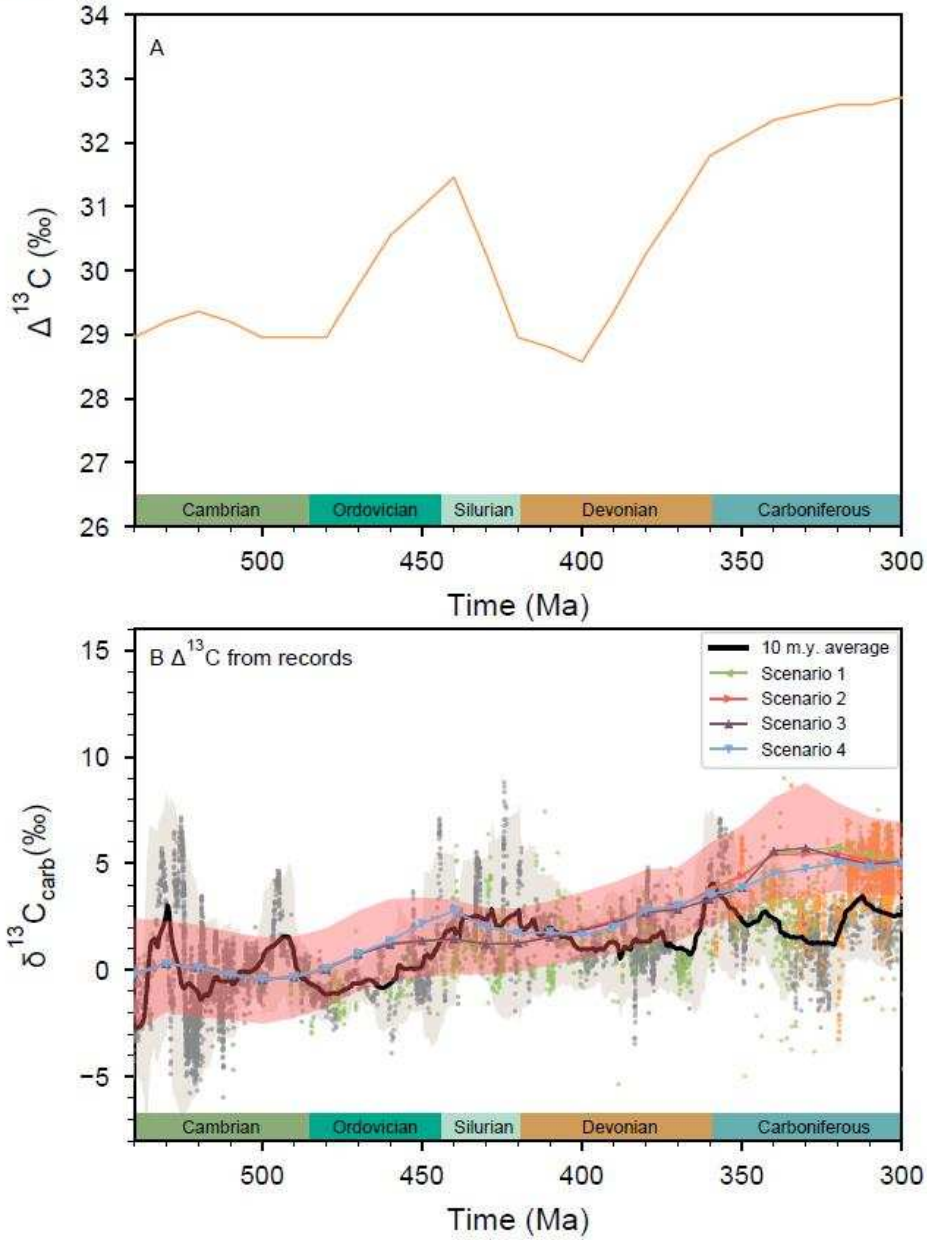
A
Δ13C (‰)
34
33
32
31
30
29
28
27
26
Cambrian
Ordovician
Silurian
Devonian
Carboniferous
500
450
400
350
300
Time (Ma)
B Δ13C from records
10 m.y. average
Scenario 1
Scenario 2
Scenario 3
Scenario 4
δ13Ccarb (‰)
15
10
5
0
−5
Cambrian
Ordovician
Silurian
Devonian
Carboniferous
500
450
400
350
300
Time (Ma)

563

Fig. 10

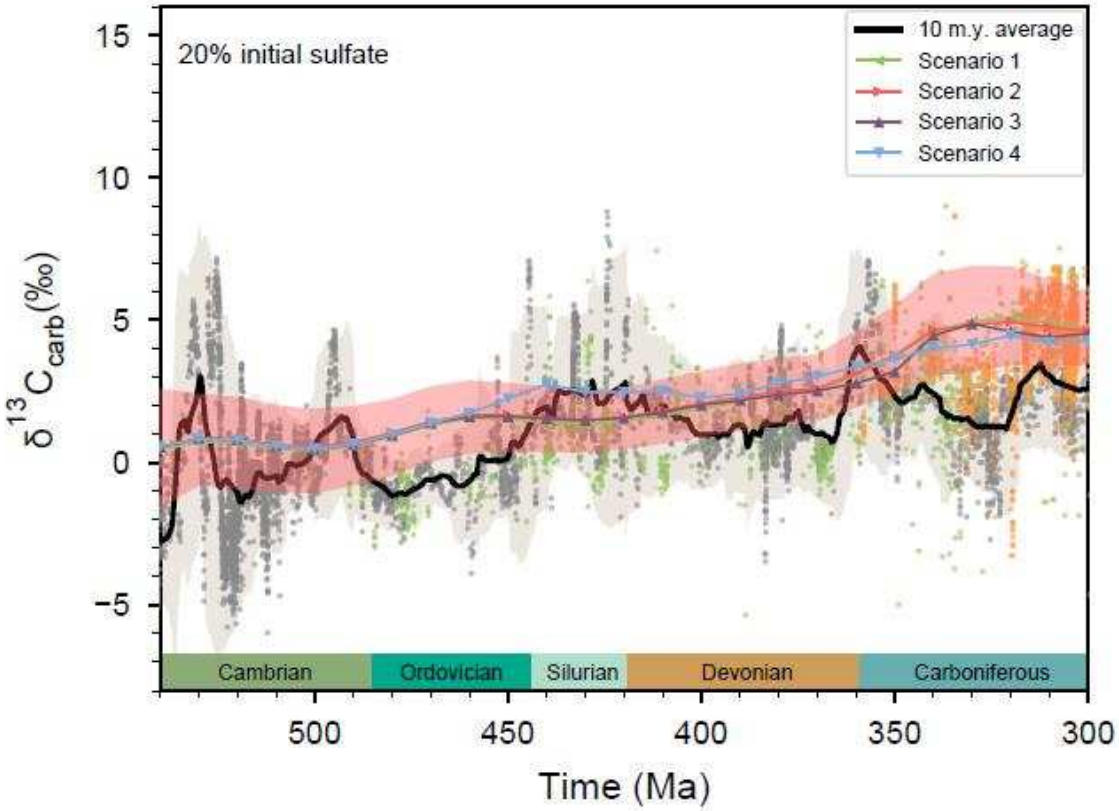
20% initial sulfate
10 m.y. average
Scenario 1
Scenario 2
Scenario 3
Scenario 4
15
10
5
0
−5
δ13Ccarb(‰)
Cambrian
Ordovician
Silurian
Devonian
Carboniferous
500
450
400
350
300
Time (Ma)

564

Fig. 11

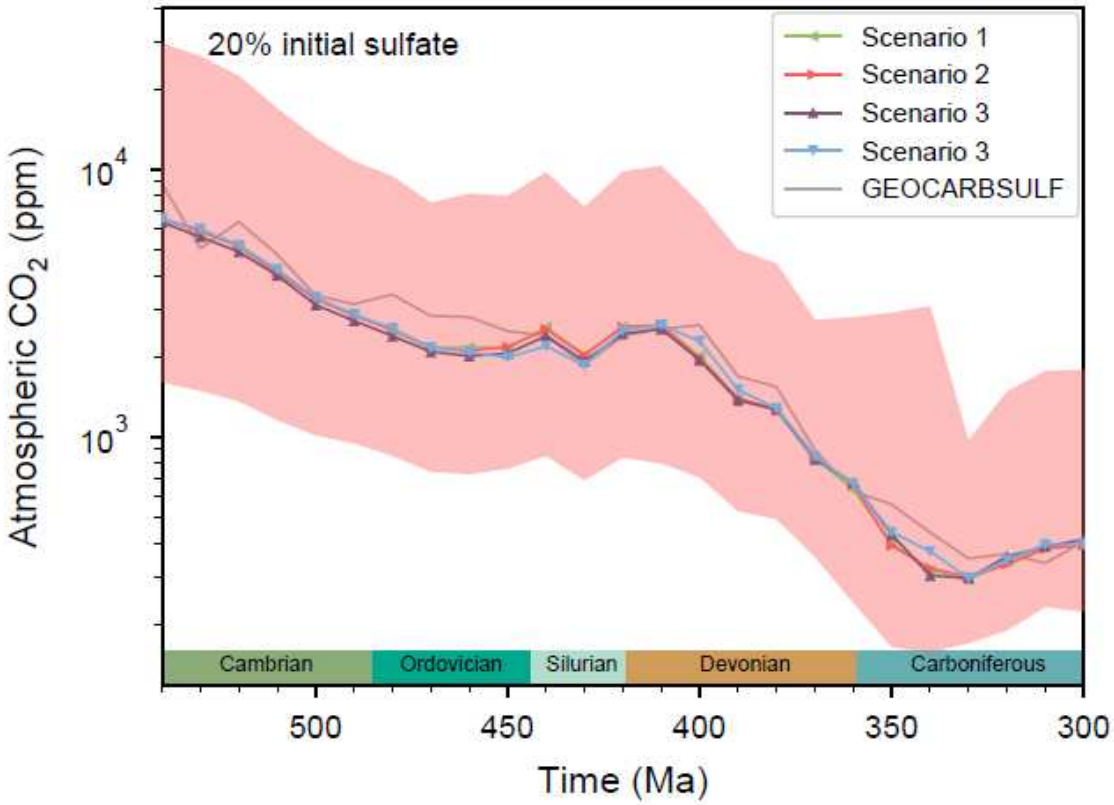
20% initial sulfate
Scenario 1
Scenario 2
Scenario 3
Scenario 3
GEOCARBSULF
Atmospheric CO_2 (ppm)
10^4
10^3
Cambrian
Ordovician
Silurian
Devonian
Carboniferous
500
450
400
350
300
Time (Ma)

565